DOI: 10.17725/j.rensit.2024.16.101

Optimization of optical absorption in spintronic terahertz emitters using Bragg reflectors

Anastasiya V. Gorbatova, Arseny M. Buryakov

MIREA - Russian technological university, https://www.mirea.ru/

Moscow 119454, Russian Federation

E-mail: gorbatova@mirea.ru, buryakov@mirea.ru

Received October 21, 2023, peer-reviewed October 25, 2023, accepted October 31, 2023, published March 15, 2024.

Abstract: **An optimized design of a spintronic terahertz emitter has been developed, based on a bilayer Co/Pt structure with an integrated distributed Bragg reflector. The incorporation of the Bragg mirror between the Co/Pt structure and the silicon substrate enhances optical absorption in the ferromagnetic layer, thereby amplifying spin current generation and, consequently, THz signal. A model was developed for calculating the optical absorption in the ferromagnetic layer of the spintronic emitter, taking into account the parameters of the Bragg mirror (layer thicknesses, period) based on the superlattice structure [TiO_2/SiO_2] N. This model is grounded on the solution of Maxwell's equations for electromagnetic waves using the COMSOL Multiphysics software. The effect of anti-reflective dielectric coatings on the level of optical absorption in the ferromagnetic layer was also analyzed. The study confirmed that using the optimized Bragg mirror is sufficient for achieving optimal absorption.**

Keywords: **terahertz radiation, spintronic emitter, Bragg mirror, anti-reflection coating, Fabry-Perot cavity, COMSOL Multiphysics**

UDC 535.34, 537.9

Acknowledgments: The study was supported by the Russian Science Foundation Grant No. 21-79-1035, https://rscf.ru/en/project/21-79-10353/

For citation: Anastasiya V. Gorbatova, Arseny M. Buryakov. Optimization of optical absorption in spintronic terahertz emitters using Bragg reflectors. *RENSIT: Radioelectronics. Nanosystems. Information Technologies,* 2024, 16(1):101-110e. DOI: 10.17725/j.rensit.2024.16.101.

Contents

1. INTRODUCTION

Terahertz (THz) radiation in the 0.1-30 THz range represents an effective means for spectroscopic analysis, opening new horizons in condensed matter physics research, including studies of phonon and magnon modes, as well as electronic and spin dynamics [1-4]. Consequently, there is a growing demand for high-power and broadband terahertz emitters capable of exciting a variety of physical processes in solids. Among THz emitters, the most well-known and utilized in THz spectrometers are nonlinear optical crystals, such as $LiNbO_3$, ZnTe, and GaP [5], organic crystals, photoconductive antennas (PCAs), and spintronic terahertz emitters (STEs) [5,6]. The first two types of sources operate on the basis of nonlinear optical rectification [5-7], while the latter two rely on ultrafast current generation [8,9]. Most

nonlinear optical crystals generate THz pulses with peak field strengths around 100 kV/cm [5,6]. An exception is $LiNbO_3$, which, when pumped with a tilted-front pulse for phase matching and at cryogenic temperatures, generates THz pulses with peak field strengths exceeding 4 MV/cm [10]. Organic crystals, such as BNA, also facilitate the generation of THz pulses with high electric field strengths, approximately 1-10 MV/cm, across spectral widths from 1 to 10 THz [5,6]. However, their stability depends on the optical pumping conditions, often requiring the use of IR lasers. For generating high field strengths in THz pulses, nonlinear optical and organic crystals are frequently used in combination with pumping lasers with powers of several tens of mJ. In contrast, PCAs do not require large energies, but their field strength rarely exceeds 100 kV/cm [5,6].

In recent years, special attention has been devoted to spintronic terahertz emitters, which operate on the principle of spin-charge conversion [8]. According to the 2023 roadmap, THz spintronics introduces new functional capabilities for THz photonics in the generation, modulation, and detection of THz radiation [11]. The classical design of STEs consists of a bilayer (or trilayer) structure based on ferromagnetic (FM) and non-magnetic metals (NM): FM/NM or NM($\pm\gamma$)/FM/NM($\mp\gamma$), where γ signifies the sign of the Spin Hall angle [12]. The film thickness within the structure does not exceed a few nanometers ($\sim 2-3$ nm) [12]. The operating principle of STEs includes four fundamental stages [13]:

1. Absorption of the optical pulse from laser pumping.
2. Generation of spin current in the magnetic layer and its transfer to the non-magnetic layer.
3. Conversion of spin current into a transverse charge current.
4. Operation of STE as a source of THz electromagnetic pulses.

STE devices are characterized by their simple architecture, high manufacturability, and the generation of THz pulses with significant amplitudes, spanning from 100 kV/cm to 1.5 MV/cm. Additionally, these devices operate across a broad frequency range of 0.1 to 30 THz [6]. Another key benefit is the capacity for fine-tuning parameters of THz radiation, such as polarization, ellipticity, amplitude, and frequency range [14-18].

Despite the many advantages of STEs, their low absorption of optical and near-infrared (IR) pump radiation leads to inefficient optical-THz conversion. This issue primarily stems from the minimal thickness of standard STEs. To date, considerable efforts have been directed toward enhancing these parameters, including modifying STEs' functional layers (material type, thickness, etc.) [12,19-21], adopting cascade amplification schemes for THz radiation [22], and amplifying THz radiation through the creation of hybrid structures. These structures combine spin-charge conversion approaches with the development of antennas on the surface of STE films [18,23]. Additionally, the application of plasmonic approaches and the creation of microstructured STEs [24-26], as well as the establishment of conditions for resonant absorption of optical radiation in STEs' functional structure via the integration of dielectric (Bragg) mirrors [27,28], have been explored. Among all these approaches, the last appears to be the simplest from a technological standpoint. Furthermore, alongside Bragg mirrors, the use of anti-reflection coatings (ARCs) operating in the IR range, which also serve a protective function, can reduce the loss of exciting radiation upon reflection from the air/STE interface.

This study focuses on optimizing STE with Co/Pt layers to enhance optical absorption in the ferromagnetic cobalt layer. Employing numerical simulations within the COMSOL Multiphysics

software package, two strategies were examined to maximize the absorption of pump radiation in the functional layer of STE: 1) the construction of Bragg mirrors, serving as analogues to optical resonators between the STE and the substrate; and 2) the application of anti-reflective coatings on the surface of STEs.

2. MODEL OF A THZ GENERATOR WITH A BRAGG MIRROR AND ANTI-REFLECTIVE COATING

The concept of developing a STE with a Bragg mirror hinges on the fundamental processes of THz radiation generation. Among these, a crucial step is the absorption of the optical pulse by the ferromagnetic layer within the STE heterostructure. According to formula (1), the amplitude of the generated THz wave is directly proportional to the energy absorbed from the optical excitation beam [13,29]:

$$E_{THz} \propto \frac{P_{abs}}{d_{Co}+d_{Pt}} \tanh\frac{d_{Co}+d_0}{2\lambda_{pol}} \tanh\frac{d_{Pt}}{2\lambda_{pol}} \times \times \frac{1}{n_{air}+n_{sub}+Z_0(\sigma_{Co}d_{Co}+\sigma_{Pt}d_{Pt})} e^{-\frac{d_{Co}+d_{Pt}}{S_{THz}}}, \quad (1)$$

where P_{abs} is the laser radiation power absorbed by the emitter, d_{Co} is the thickness of the ferromagnetic cobalt layer, d_{Pt} is the thickness of the non-magnetic platinum layer, d_0 is the critical value of the thickness of the ferromagnetic layer, below which the ferromagnetic layer loses its magnetic properties, λ_{pol} is the characteristic spin polarization constant that appears in case when $d > d_0$, n_{air}, n_{sub} and Z_0 – are the refractive index of air, the refractive index of the substrate at THz frequencies and the vacuum impedance, respectively, σ_{Co} and σ_{Pt} – denote the electrical conductivity of the two materials, respectively, S_{THz} is the effective inverse attenuation coefficient of THz radiation in both metal layers. Note that the simplified formula does not take into account the spin and charge components [13,29].

Addressing the issue of optimizing the absorption capacity of the Spintronic Terahertz Emitter (STE) structure, we delve into the operational principles and characteristics of the Bragg mirror. This mirror features a periodic structure composed of two materials with differing refractive indices. The optimal number of periods in a Bragg mirror for achieving maximum reflection is dictated by the difference in the refractive indices of two dielectric materials: $\Delta n/n = (n_H - n_L)/n_H$, where H and L denote the materials with high and low refractive indices, respectively. The Bragg mirror achieves 100% reflection of incident radiation at the central wavelength $\lambda_p = 2(n_H d_H + n_L d_L)$, with d representing the layer thickness. Optimal reflection efficiency occurs when the thicknesses of the individual layers are equal to a quarter wavelength, $n_H d_H = n_L d_L = \lambda_p/4$. The quality factor of the resonator is defined as $Q = f/\Delta f$, where f and Δf are the frequency and the frequency peak width, respectively [30]. In the STE context, an experimental deployment of a Bragg mirror is documented in [27]. In this study, a Bragg structure [TiO_2 (113 nm, n = 2.265)|SiO_2 (185 nm, n = 1.455)]$_5$ optimized for a pump wavelength of approximately 1030 nm was incorporated into a three-layer W/CoFeB/Pt spintronic emitter. This integration resulted in the electric field in the THz range being doubled and a fourfold increase in power. Another study [28] demonstrated a performance enhancement of SSCs optically pumped at 800 nm by up to sixfold, attributable to the [SiO_2 (165 nm) TiO_2 (94 nm)]$_5$ structure. Hence, the creation of an optical resonator can significantly boost the absorption within the STE structure, which, in turn, facilitates an increase in THz power output.

Optimizing the properties of the Bragg mirror is critical to improve optical pump absorption. However, to ensure optimal transmission of optical pumping through the STE, creating conditions for complete "anti-reflection" at the air/STE interface using ARCs is equally important. Two primary criteria must be satisfied to achieve this condition [31]. First, the waves

reflected from the structure's surface and from the interface should have a phase difference of $\delta = n\pi/2$, where n is the refractive index of the film. Second, the film thickness (d) must be an odd multiple of $i\lambda/4$, where λ is the wavelength of the incident beam and i is an odd positive integer. ARCs can be either homogeneous, consisting of one uniform layer with refractive index n, or inhomogeneous, comprising layers with a gradient of n in each layer.

To ensure total reflection conditions when using an ARC source, the refractive index must equal $n = \sqrt{n_{air} n_s}$, where n_s is the refractive index of the substrate, and the thickness of the ARC (h_{ARC}) should be a quarter of the wavelength. Single-layer homogeneous ARCs are utilized to suppress reflectance down to 2.5% across a broad spectral range (450–1100 nm) at normal incidence. Examples of single-layer ARCs for the visible and IR ranges include MgF_2, SiO_2, Si_3N_4, Al_2O_3, TiO_2, etc. To further reduce reflectance, two-layer ARCs can be employed. A necessary condition for achieving zero reflectance with a two-layer coating, where both layers have the same optical thickness ($n_1 d_1 = n_2 d_2 = \lambda/4$), is that the product of their refractive indices meets the relationship $n_1 n_2 = n_0 n_s$ [31].

This work introduces a model of a classical Spintronic Terahertz Emitter (STE), comprising a two-layer structure (**Fig. 1***a*). Both layers, made of Co and Pt, share the same thickness of 2 nm. The selection of these thickness values, $d_{Co} = d_{Pt}$, was determined by the optimal balance between the critical thickness of the ferromagnetic layer, d_0, and the effective attenuation coefficient for THz radiation, S_{THz}, in both metal layers. A consensus among most experimental and theoretical studies suggests that maximal THz generation is attained in a two-layer STE structure with an overall thickness of 4 nm [12,29]. Subsequently, a Bragg mirror, forming a superlattice of the $[SiO_2|TiO_2]_N$ type where N varies as 1, 3, 5, and 10, is inserted between the STE and the high-resistivity silicon substrate (illustrated in Fig. 1*b*). This high-resistivity silicon

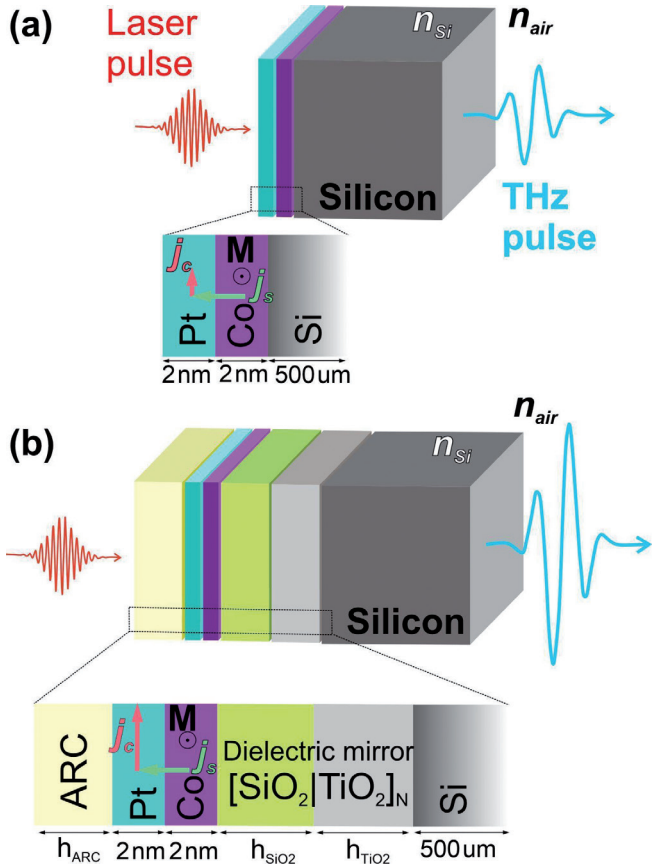

Fig. 1. *(a) STE structure fabricated on a silicon substrate. (b) STE design incorporating a Bragg mirror, constructed on a silicon substrate, and equipped with an anti-reflection coating.*

substrate was selected for its superior THz radiation transmission capability ($n\mathrm{Si}_{THz} \approx 3.4$, significantly greater than $n_{air} \approx 1$). Fig. 1*a* depicts the configuration of the STE without a Bragg mirror, whereas Fig. 1*b* displays the schematic with a Bragg mirror. An anti-reflection coating (ARC) was applied to shield the surface of the STE from external factors and to enhance radiation transmission.

The COMSOL Multiphysics software platform was utilized for calculating the absorption in a STE based on a Co/Pt bilayer structure. Through the physical interface "Optics" > "Wave Optics" > "Electromagnetic Waves, Frequency Domain", it is possible to ascertain the distribution of the electromagnetic field within the medium by solving Maxwell's equation for an electromagnetic wave:

$$\nabla \times \mu_r^{-1}\left(\nabla \times \vec{E}\right) - k_0^2\left(\varepsilon_r - \frac{j\lambda\sigma}{2\pi c\varepsilon_0}\right)\vec{E} = 0, \qquad (2)$$

where μ_r and ε_r are the magnetic and dielectric constants of the material, respectively, σ is its conductivity, ε_0 is the vacuum permittivity, k_0 is the wave number, λ is the wavelength of the pump radiation, c is the speed of light in a vacuum, and $\vec{E}$ is the complex vector of the electric field.

The simulation of the electromagnetic wave was executed with the "Port" boundary condition, where the electric field strength vector is oriented along the X-axis, and its amplitude was set at 1 V/m. To the side boundaries of the model, the "Perfect Electric Conductor" boundary condition was applied, enforcing the condition $\vec{n} \times \vec{E} = 0$.

3. RESULTS AND DISCUSSION

In the initial stage, the most basic version of the structure depicted in Fig. 1*a* is examined, absent both a Bragg mirror and ARC. It is important to highlight that silicon substrates are invariably characterized by a thin layer of natural oxide, SiO_2, on their surface. The absorption of optical radiation at a wavelength of 800 nm in the SiO_2 layer is relatively low (extinction coefficient k_{SiO2} = 0.000687 [32]). However, considering that the refractive index of the oxide is n_{SiO2} = 1.4574 [32], and the SiO_2 layer is situated between the STE structure and the silicon substrate, which exhibits high refractive indices in the IR range (n_{Co} = 4.56, n_{Pt} = 6.57 [33], and n_{Si} = 3.6690) [34]), this configuration leads to multipath interference. This structure acts as the simplest form of an optical resonator and can circumvent the need for more complex designs to moderately suppress back reflection. By adjusting the thickness of the oxide layer, an enhancement in optical absorption can be achieved, which may also contribute to an increase in the THz signal.

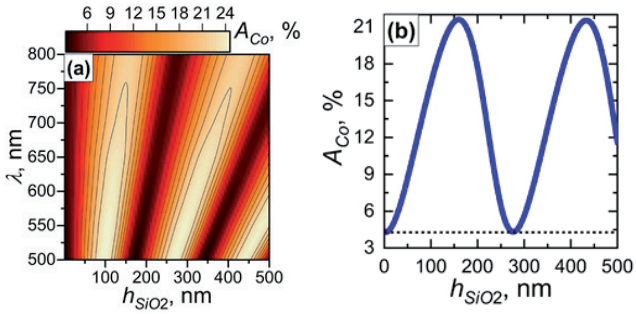

Fig. 2. *Impact of SiO_2 layer thickness on optical absorption in STE based on the Pt (2 nm)/Co (2 nm) structure. (a) Distribution map of absorption in STE across optical and near-IR pump wavelength ranges. (b) Relationship between absorption in the ferromagnetic layer and SiO_2 thickness at a wavelength of 800 nm.*

The results depicted in **Fig. 2***a* and *b* illustrate a map of optical absorption in the ferromagnetic cobalt layer (A_{Co}) as a function of the SiO_2 thickness and the wavelength of the exciting radiation (500-800 nm). As shown in the figures, for cases with a minimum natural oxide thickness of ~ 1-2 nm, the absorption at these wavelengths is approximately 4.3%. However, as the oxide thickness increases, the maximum absorption shifts towards the 500 nm region, potentially reaching up to 24% of the total exciting radiation. When considering a wavelength of 800 nm (Fig. 2*b*) – the operational range for most available femtosecond laser systems used to pump THz STEs – the absorption does not exceed 21.6% for an oxide thickness of ~ 160 nm. In this scenario, the resultant total absorption ratio for Co(2 nm)/Pt(2 nm) is approximately 52.5%, with the proportion of reflected light being around 7.6%. The remaining excitation radiation, 39.3%, passes through the STE and is absorbed by the SiO_2/Si substrate.

This example underscores the ineffectiveness of a SiO_2 film alone, situated between the STE's functional structure and the silicon substrate, in achieving maximum absorption. Consequently, in the subsequent stage, the focus shifted to an STE structure enhanced by a Bragg mirror, utilizing the $[SiO_2|TiO_2]_N$ superlattice configuration. The

pairing of SiO_2 layers with TiO_2 layers, which have markedly distinct refractive indices at a wavelength of 800 nm (n_{TiO2} = 2.0951, n_{SiO2} = 1.4608) [32,35], facilitates a reduction in the fraction of radiation transmitted into the substrate. The primary goal for achieving maximum absorption in STE involves determining the optimal period N for the $[SiO_2|TiO_2]_N$ structure, along with the optimal thicknesses for each dielectric layer. **Fig. 3***a-d* showcase the results from calculating the absorption efficiency in the cobalt layer for various N values (1, 3, 5, 10), considering SiO_2 layer thicknesses in the range of 1-300 nm and TiO_2 layer thicknesses also within 1-300 nm.

From the analysis of the data presented, it is clear that the structure with a single period $[SiO_2|TiO_2]$ does not offer a significant enhancement in absorption compared to the previously considered Pt/Co/SiO_2(160nm)/Si configuration. The maximum absorption in the Co layer is capped at 21.6% (Fig. 3*a*). However, as the periodicity of the Bragg mirror increases, so does the absorption in the STE. For N = 3 (Fig. 3*b*), the absorption maximum increases to 27.5%. Considering the structure $[SiO_2(145\ нм)|TiO_2(105\ нм)]_5$ (Fig. 3*c*), similar to the one studied in [28], the peak absorption in the ferromagnetic layer achieves approximately 35%. With an increment in the number of periods to 10 in the $[SiO_2(160\ нм)|TiO_2(95\ нм)]_{10}$ configuration, the absorption in the Co layer rises to approximately 39% (Fig. 3*d*). Further increases in the number of superlattice periods become impractical, as the total absorption in the STE (accounting for both the cobalt and platinum layers) at 10 superlattice periods approaches approximately 97%.

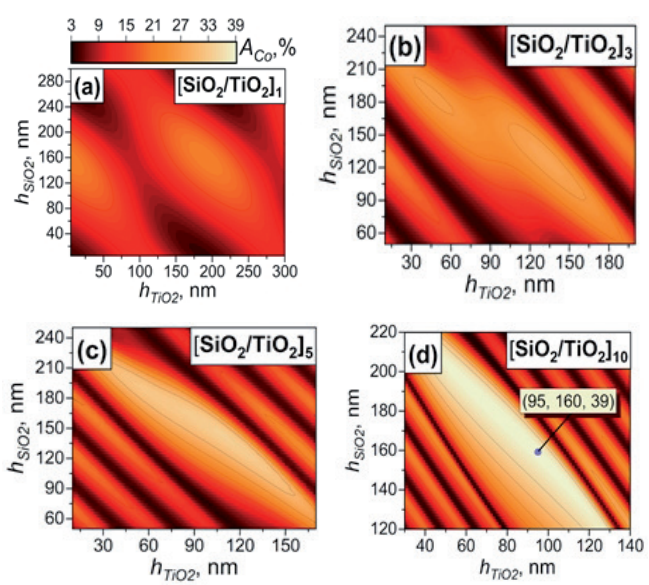

Fig. 3. *Dependence of absorption in the cobalt layer of an STE with a Bragg mirror $[SiO_2|TiO_2]N$ on the thicknesses of the dielectric layers h_{SiO2} and h_{TiO2} and the structure period N: N = 1 (a), N = 3 (b), N = 5 (c), N = 10 (d).*

To achieve maximum absorption efficiency in the cobalt A_{Co} layer, further calculations were conducted for the optimized structure $[SiO_2(160\ нм)|TiO_2(95\ нм)]_{10}$. These calculations incorporated the application of an anti-reflection coating to the STE structure, as depicted in Fig. 1*b*. The selection of a material for such a coating is pivotal, necessitating the right refractive index and optimal thickness for efficient performance at a wavelength of 800 nm. Our research evaluated a broad spectrum of materials commonly utilized as anti-reflection coatings in the near-infrared region. The materials considered, along with their characteristic refractive indices n at a wavelength of 800 nm and references to literature sources, are listed in **Table 1.**

Table 1

Materials for Anti-Reflection Coatings in the Visible and IR Wavelength Ranges

Material	*n*	Source
MgF_2	1.4194	[36]
SiO_2	1.4574	[32]
MgO	1.7276	[37]
Al_2O_3	1.6710 1.75	[38] [39]
HfO_2	1.9809	[40]
Si_3N_4	1.9962	[41]
Ta_2O_5	2.0719 2.1594	[32] [42]
TiO_2	2.0951	[35]

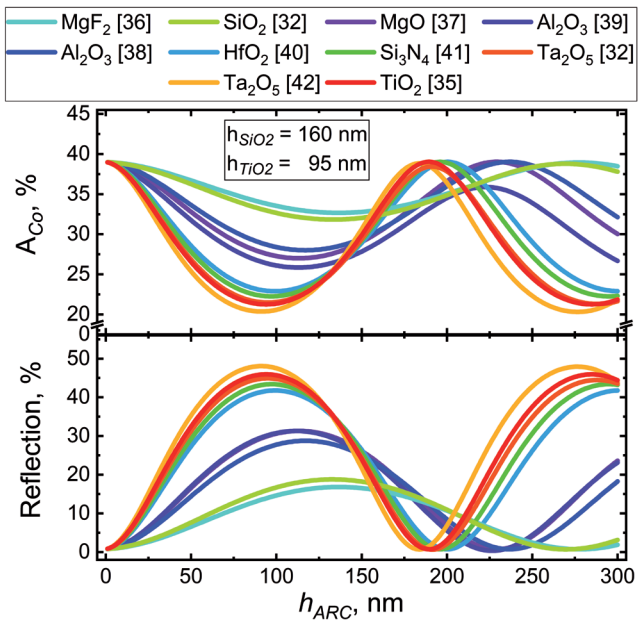

Fig. 4. *Absorption and reflection characteristics for an STE based on Pt(2 nm)/Co(2 nm) with a Bragg grating* $[SiO_2(160\ nm)|TiO_2(95\ nm)]_{10}$ *and with an anti-reflection coating.*

Fig. 4 presents the results of a comprehensive analysis of reflection and absorption of 800 nm wavelength radiation in the STE Pt(2 nm)/Co(2 nm), conducted based on the type of anti-reflection coating material (see Table 1) and the thickness of this coating.

Based on our calculations, we concluded that employing an anti-reflection coating does not result in a significant increase in absorption within the cobalt layer. This outcome aligns with previous findings indicating that the absorption efficiency in an STE, when using a Bragg mirror with $N = 10$, approaches 100%. At the minimum thickness of the ARC for all considered materials, a peak absorption in the cobalt layer is observed (see Fig. 4). This corroborates the efficiency of the optimized Bragg mirror design in effectively absorbing radiation traversing the structure.

Although various types of ARCs are ineffective in enhancing absorption and cannot fulfill their primary function in this context, their high resistance to external factors allows them to serve as conventional protective coatings. The thickness of the protective layer can be optimized so as not to detrimentally impact the optical properties or reduce the efficiency of pump laser radiation absorption. From the data presented in Fig. 4, three key groups of materials used in the simulations emerge: 1) TiO_2, Ta_2O_5, Si_3N_4, and HfO_2; 2) MgO and Al_2O_3; and 3) SiO_2 and MgF_2. Materials in the first group exhibit the most pronounced absorption minima at a characteristic thickness of 90 nm, achieving absorption up to ~ 20% and reflection ~ 50%. Conversely, materials in the second group display more gradual absorption minima, with absorption reaching ~ 25% at a characteristic layer thickness of ~ 115 nm. The third group's materials are the least sensitive to thickness changes, showing a minimum absorption of ~ 32% at a characteristic thickness of ~ 137 nm. Therefore, different ARC materials possess distinct characteristics that must be considered when selecting the most appropriate protective coating for a specific optical application.

4. CONCLUSION

The study developed a model of a spintronic terahertz emitter integrated with Bragg mirrors, structured as a $[SiO_2(160\ nm)|TiO_2(95\ nm)]_N$ superlattice, where N denotes the number of periods. The investigation revealed that with N equal to 10, the developed model achieves maximum optical absorption in the cobalt layer, reaching approximately 39%. Simultaneously, the total absorption in the STE structure approaches 100%. This marks a significant increase, over ninefold, compared to the absorption in the non-optimized Co(2 nm)/Pt(2 nm) structure on a high-resistivity silicon substrate, initially at only 4.3%. These findings are crucial as they underscore the potential of employing optical resonators, such as Bragg mirrors, to significantly enhance optical-terahertz conversion in STE structures and optimize laser pump powers. Additionally, it was discovered that even a relatively simple STE/SiO_2/Si system with an optimized oxide layer thickness of 160 nm can enhance absorption by approximately fivefold.

Further analysis indicated that the application of anti-reflection coatings does not result in an additional increase in absorption within the ferromagnetic layer of the optimized structure incorporating a Bragg mirror [SiO_2(160 nm)|TiO_2(95 nm)]. Nonetheless, it is essential to acknowledge that the inclusion of reflective coatings, such as MgF_2 and SiO_2, does not impair the absorption and reflectance characteristics of the structure, thereby allowing their consideration as protective layers based on specific requirements.

In conclusion, the significance of an integrated approach in designing STE structures is emphasized, encompassing not only the optimization of the ferromagnetic layer but also the incorporation of additional optical elements, such as dielectric superlattices and protective coatings. This comprehensive strategy enhances the understanding of light interaction processes with these structures and paves the way for the development of highly efficient devices in the realms of terahertz electronics and spintronics.

REFERENCES

1. Kubacka T, Johnson JA, Hoffmann MC, Vicario C, de Jong S, Beaud P, Grübel S, Huang S-W, Huber L, Patthey L, Chuang Y-D, Turner JJ, Dakovski GL, Lee W-S, Minitti MP, Schlotter W, Moore RG, Hauri CP, Koohpayeh SM, Scagnoli V, Ingold G, Johnson SL, Staub U. Large-Amplitude Spin Dynamics Driven by a THz Pulse in Resonance with an Electromagnon. *Science,* 2014, 343(6177):1333-1336.
2. Blank TGH, Grishunin KA, Mashkovich EA, Logunov MV, Zvezdin AK, Kimel AV. THz-Scale Field-Induced Spin Dynamics in Ferrimagnetic Iron Garnets. *Phys. Rev. Lett.,* 2021, 127(3):037203.
3. Mikhaylovskiy RV, Hendry E, Kruglyak VV, Pisarev RV, Rasing T, Kimel AV. Terahertz emission spectroscopy of laser-induced spin dynamics in $TmFeO_3$ and $ErFeO_3$ orthoferrites. *Phys. Rev. B.*, 2014, 90(18):184405.
4. Zhang W, Maldonado P, Jin Z, Seifert TS, Arabski J, Schmerber G, Beaurepaire E, Bonn M, Kampfrath T, Oppeneer PM, Turchinovich D. Ultrafast terahertz magnetometry. *Nat. Commun.*, 2020, 11(1):4247.
5. Fülöp JA, Tzortzakis S, Kampfrath T. Laser-Driven Strong-Field Terahertz Sources. *Adv. Opt. Mater.*, 2020, 8(3):1900681.
6. Bilyk VR, Brekhov KA, Agranat MB, Mishina ED. Dispersion of optical constants of Si:PbGeO crystal in the terahertz range. *Russian Technological Journal,* 2023, 11(3):38-45; doi: 10.32362/2500-316X-2023-11-3-38-45.
7. Blanchard F, Razzari L, Bandulet HC, Sharma G, Morandotti R, Kieffer JC, Ozaki T, Reid M, Tiedje HF, Haugen HK, Hegmann FA. Generation of 1.5 μJ single-cycle terahertz pulses by optical rectification from a large aperture ZnTe crystal. *Opt. Express*, 2007, 15(20):13212.
8. Feng Z, Qiu H, Wang D, Zhang C, Sun S, Jin B, Tan W. Spintronic terahertz emitter. *J. Appl. Phys.*, 2021, 129(1):010901.
9. Lepeshov S, Gorodetsky A, Krasnok A, Rafailov E, Belov P. Enhancement of terahertz photoconductive antenna operation by optical nanoantennas. *Laser Photon. Rev.*, 2017, 11(1):1600199.
10. Wu X, Ma J, Zhang B, Chai S, Fang Z, Xia C-Y, Kong D, Wang J, Liu H, Zhu C-Q, Wang X, Ruan C-J, Li Y-T. Highly efficient generation of 0.2 mJ terahertz pulses in lithium niobate at room temperature with sub-50 fs chirped Ti:sapphire laser pulses. *Opt. Express*, 2018 26(6):7107.
11. Leitenstorfer A, Moskalenko AS, Kampfrath T, Kono J, Castro-Camus E, Peng K, Qureshi N, Turchinovich D, Tanaka K, Markelz AG, Havenith M, Hough C, Joyce HJ, Padilla WJ, Zhou B, Kim K-Y, Zhang X-C, Jepsen PU, Dhillon S, Vitiello M, Linfield E, Davies AG, Hoffmann MC, Lewis R, Tonouchi M, Klarskov P, Seifert TS, Gerasimenko YA, Mihailovic D, Huber R, Boland JL, Mitrofanov O, Dean P, Ellison BN, Huggard PG, Rea SP, Walker C, Leisawitz DT, Gao JR, Li C, Chen Q, Valušis G, Wallace VP, Pickwell-MacPherson E, Shang X, Hesler J, Ridler N, Renaud CC, Kallfass I, Nagatsuma T, Zeitler JA, Arnone D, Johnston MB, Cunningham J. The 2023 terahertz science and technology roadmap. *J. Phys. D. Appl. Phys.*, 2023, 56(22):223001.

12. Seifert T, Jaiswal S, Martens U, Hannegan J, Braun L, Maldonado P, Freimuth F, Kronenberg A, Henrizi J, Radu I, Beaurepaire E, Mokrousov Y, Oppeneer PM, Jourdan M, Jakob G, Turchinovich D, Hayden LM, Wolf M, Münzenberg M, Kläui M, Kampfrath T. Efficient metallic spintronic emitters of ultrabroadband terahertz radiation. *Nat. Photonics,* 2016, 10(7):483-488.
13. Seifert TS, Cheng L, Wei Z, Kampfrath T, Qi J. Spintronic sources of ultrashort terahertz electromagnetic pulses. *Appl. Phys. Lett.*, 2022, 120(18):180401.
14. Khusyainov D, Ovcharenko S, Gaponov M, Buryakov A, Klimov A, Tiercelin N, Pernod P, Nozdrin V, Mishina E, Sigov A, Preobrazhensky V. Polarization control of THz emission using spin-reorientation transition in spintronic heterostructure. *Sci. Rep.*, 2021, 11(1):697.
15. Lezier G, Koleják P, Lampin J-F, Postava K, Vanwolleghem M, Tiercelin N. Fully reversible magnetoelectric voltage controlled THz polarization rotation in magnetostrictive spintronic emitters on PMN-PT. *Appl. Phys. Lett.*, 2022, 120(15):152404 .
16. Khusyainov D, Ovcharenko S, Buryakov A, Klimov A, Pernod P, Nozdrin V, Mishina E, Sigov A, Preobrazhensky V, Tiercelin N. Composite Multiferroic Terahertz Emitter: Polarization Control via an Electric Field. *Phys. Rev. Appl.,* 2022, 17(4):044025.
17. Buryakov AM, Gorbatova AV, Avdeev PY, Lebedeva ED, Brekhov KA, Ovchinnikov AV, Gusev NS, Karashtin EA, Sapozhnikov MV, Mishina ED, Tiercelin N, Preobrazhensky VL. Efficient Co/Pt THz spintronic emitter with tunable polarization. *Appl. Phys. Lett.*, 2023, 123(8):082404.
18. Chen M, Wu Y, Liu Y, Lee K, Qiu X, He P, Yu J, Yang H. Current-Enhanced Broadband THz Emission from Spintronic Devices. *Adv. Opt. Mater.*, 2019, 7(4):1801608.
19. Buryakov A, Avdeev P, Khusyainov D, Bezvikonnyy N, Coclet A, Klimov A, Tiercelin N, Lavrov S, Preobrazhensky V. The Role of Ferromagnetic Layer Thickness and Substrate Material in Spintronic Emitters. *Nanomaterials,* 2023, 13(11):1710.
20. Buryakov A, Gorbatova A, Avdeev P, Bezvikonnyi N, Abdulaev D, Klimov A, Ovcharenko S, Mishina E. Controlled Spintronic Emitter of THz Radiation on an Atomically Thin WS2/Silicon Substrate. *Metals,* 2022, 12(10):1676.
21. Khusyainov D, Guskov A, Ovcharenko S, Tiercelin N, Preobrazhensky V, Buryakov A, Sigov A, Mishina E. Increasing the Efficiency of a Spintronic THz Emitter Based on WSe2/FeCo. *Materials,* 2021, 14(21):6479.
22. Jin Z, Peng Y, Ni Y, Wu G, Ji B, Wu X, Zhang Z, Ma G, Zhang C, Chen L, Balakin AV, Shkurinov AP, Zhu Y, Zhuang S. Cascaded Amplification and Manipulation of Terahertz Emission by Flexible Spintronic Heterostructures. *Laser Photon. Rev.,* 2022, 16(9):2100688.
23. Nandi U, Abdelaziz MS, Jaiswal S, Jakob G, Gueckstock O, Rouzegar SM, Seifert TS, Kläui M, Kampfrath T, Preu S. Antenna-coupled spintronic terahertz emitters driven by a 1550 nm femtosecond laser oscillator. *Appl. Phys. Lett.*, 2019, 115(2):022405.
24. Rathje C, von Seggern R, Meyer N, Denker C, Munzenberg M, Schafer S. Emission Properties of Structured Spintronic Terahertz Emitters. *Proc. 44th International Conference on Infrared, Millimeter, and Terahertz Waves* (*IRMMW-THz*), IEEE, 2019, pp. 1-2.
25. Liu S, Guo F, Li P, Wei G, Wang C, Chen X, Wang B, Zhao W, Miao J, Wang L, Xu Y, Wu X. Nanoplasmonic-Enhanced Spintronic Terahertz Emission. *Adv. Mater. Interfaces,* 2022, 9(2):2101296.
26. Song B, Song Y, Zhang S, Jin K, Zhu W, Li Q, Zhang Z, Lin X, Dai Y, Yan X, Ma G, Jin Z, Yao J. Controlling terahertz radiation with subwavelength blocky patterned CoFeB/Pt heterostructures. *Appl. Phys. Express,* 2019, 12(12):122003.
27. Herapath RI, Hornett SM, Seifert TS, Jakob G, Kläui M, Bertolotti J, Kampfrath T, Hendry E. Impact of pump wavelength on terahertz emission of a cavity-enhanced spintronic trilayer. *Appl. Phys. Lett.*, 2019, 114(4):041107.
28. Rouzegar R, Chekhov AL, Behovits Y, Serrano BR, Syskaki MA, Lambert CH, Engel D, Martens U, Münzenberg M, Wolf M, Jakob G, Kläui M, Seifert TS, Kampfrath T. Broadband Spintronic Terahertz Source with Peak Electric Fields Exceeding 1.5 MV/cm. *Phys. Rev. Appl.,* 2023, 19(3):034018.

29. Torosyan G, Keller S, Scheuer L, Beigang R, Papaioannou ET. Optimized Spintronic Terahertz Emitters Based on Epitaxial Grown Fe/Pt Layer Structures. *Sci. Rep.*, 2018, 8(1):1311.
30. Yu Y, Cai J, Sun J, Zhang Z, Qin H. Fabrication and characterization of a wide-bandgap and high-Q terahertz distributed-Bragg-reflector micro cavities. *Opt. Commun.*, 2018, 426:84–88.
31. Raut HK, Ganesh VA, Nair AS, Ramakrishna S. Anti-reflective coatings: A critical, in-depth review. *Energy Environ. Sci.*, 2011, 4(10):3779.
32. Rodríguez-de Marcos LV, Larruquert JI, Méndez JA, Aznárez JA. Self-consistent optical constants of SiO_2 and Ta_2O_5 films. *Opt. Mater. Express,* 2016, 6(11):3622.
33. Carey R, Newman DM, Sandoval PAG, Thomas BWJ, Grundy PJ, Lacey ETM. Optical, magneto-optical and related properties for Pt and Co multi-layer structures. *J. Magn. Soc. Japan.*, 1991, 15(91):25-28.
34. Schinke C, Christian Peest P, Schmidt J, Brendel R, Bothe K, Vogt MR, Kröger I, Winter S, Schirmacher A, Lim S, Nguyen HT, MacDonald D. Uncertainty analysis for the coefficient of band-to-band absorption of crystalline silicon. *AIP Adv.*, 2015, 5(6):067168.
35. Sarkar S, Gupta V, Kumar M, Schubert J, Probst PT, Joseph J, König TAF. Hybridized Guided-Mode Resonances via Colloidal Plasmonic Self-Assembled Grating. *ACS Appl. Mater. Interfaces,* 2019, 11(14):13752-13760.
36. Rodríguez-de Marcos LV, Larruquert JI, Méndez JA, Aznárez JA. Self-consistent optical constants of MgF2, LaF3, and CeF3 films. *Opt. Mater. Express,* 2017, 7(3):989.
37. Stephens RE, Malitson IH. Index of refraction of magnesium oxide. *J. Res. Natl. Bur. Stand.*, 1952, 49(4):249.
38. Boidin R, Halenkovič T, Nazabal V, Beneš L, Němec P. Pulsed laser deposited alumina thin films. *Ceram. Int.,* 2016, 42(1):1177-1182.
39. Querry MR. *Optical constants*. MISSOURI UNIV-KANSAS CITY, 1985.
40. Bright TJ, Watjen JI, Zhang ZM, Muratore C, Voevodin AA. Optical properties of HfO2 thin films deposited by magnetron sputtering: From the visible to the far-infrared. *Thin Solid Films,* 2012, 520(22):6793-6802.
41. Luke K, Okawachi Y, Lamont MRE, Gaeta AL, Lipson M. Broadband mid-infrared frequency comb generation in a Si_3N_4 microresonator. *Opt. Lett.,* 2015, 40(21):4823.
42. Bright TJ, Watjen JI, Zhang ZM, Muratore C, Voevodin AA, Koukis DI, Tanner DB, Arenas DJ. Infrared optical properties of amorphous and nanocrystalline Ta_2O_5 thin films. *J. Appl. Phys.,* 2013, 114(8):083515.